Stable Surface Plasmon Resonances in Small Alumina-Embedded Silver Clusters

Murilo Moreira, Emmanuel Cottancin, Michel Pellarin, Olivier Boisron, Varlei Rodrigues, Jean Lermé, Matthias Hillenkamp

Stable Surface Plasmon Resonances in Small Alumina-Embedded Silver Clusters

Murilo H. Moreira[1,2], Emmanuel Cottancin[1], Michel Pellarin[1], Olivier Boisron[1], Varlei Rodrigues[2], Jean Lermé[1], Matthias Hillenkamp[1,2]*

[1] Institute of Light and Matter, University Lyon, University Claude Bernard Lyon 1, CNRS, UMR5306, Villeurbanne F-69622, France

[2] Institute of Physics Gleb Wataghin, State University of Campinas, Campinas, SP, 13083-970, Brazil

*matthias.hillenkamp@univ-lyon1.fr

Supporting Information

Transmission Electron Microscopy

Figure S1 shows a representative TEM image of nanoparticles fabricated under identical conditions as those used to measure the black curve in Fig. 1. The mean particle diameter is determined to 4.3 nm (Fig. S2) and the particles are very close to spherical with a mean aspect ratio of 1.16 (Fig. S3).

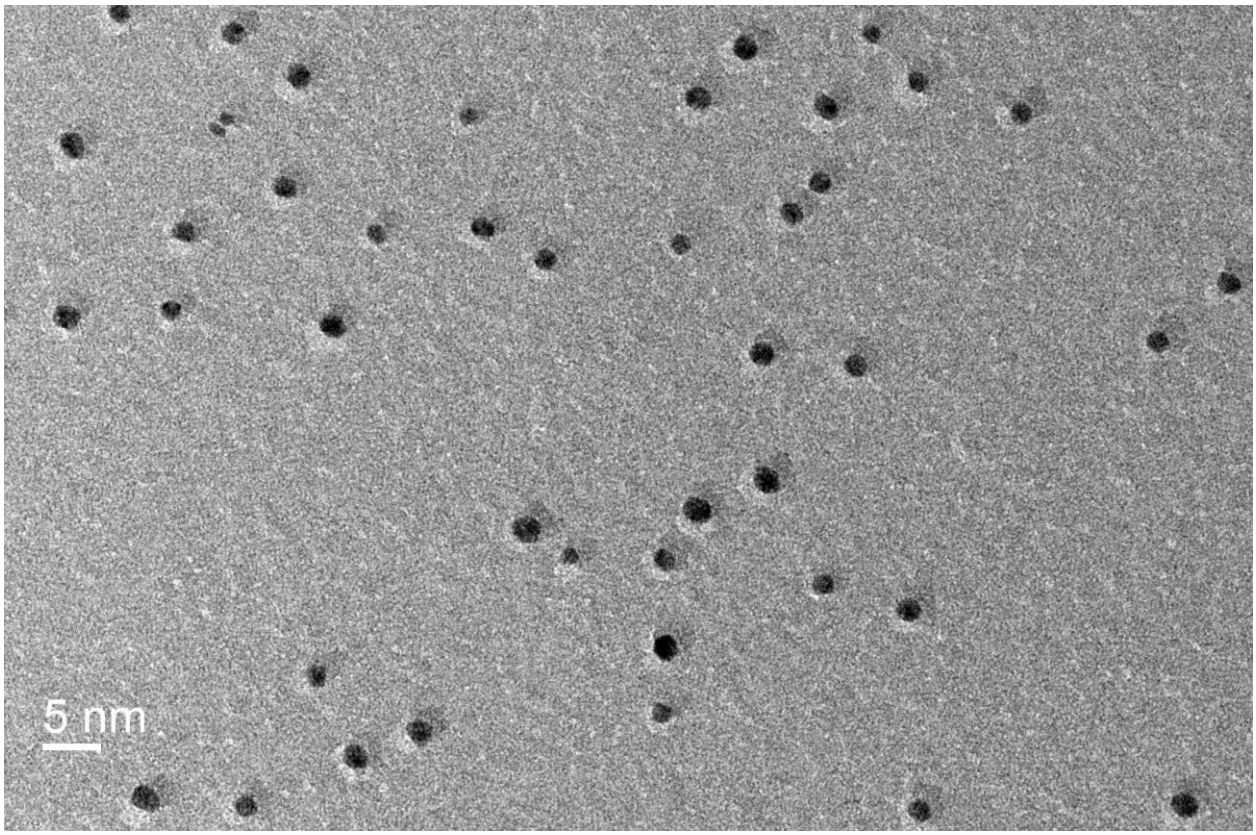

Figure S1. TEM image of alumina-embedded Ag nanoparticles corresponding to the black curve in Fig. 1.

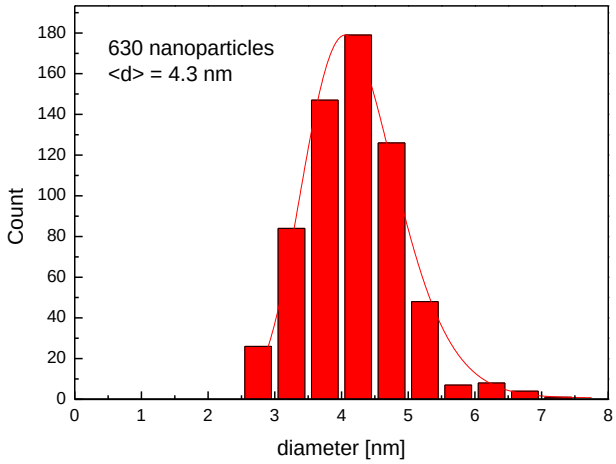

Figure S2. Diameter distribution obtained for the same sample as in Fig.S1.

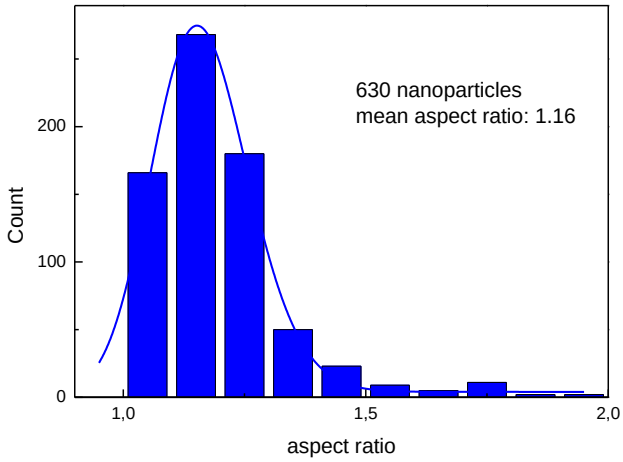

Figure S3. Aspect ratio distribution obtained for the same sample as in Fig.S1.

Numerous studies in our group over the last 25 years have shown that in general small particles are spherical and it is only above a certain, material-dependent size that ellipsoidal and ramified structures are observed [1, 2].

For the smaller nanoparticles used in this study TEM grids have been prepared and analyzed regarding the absence of coalescence. An example for mass-selected Ag NPs (n = 100-229, d = 1.5-2.0 nm) is given in Fig. S4. For these small sizes it is much more difficult to obtain images of sufficient resolution, notably due to the oxide matrix which can deteriorate under the electron beam. Such beam damage is visible in Fig. S4 in the center right. The obtained size distribution is consistent with the mass selection, within the limits of TEM image precision, as shown in Fig. S5.

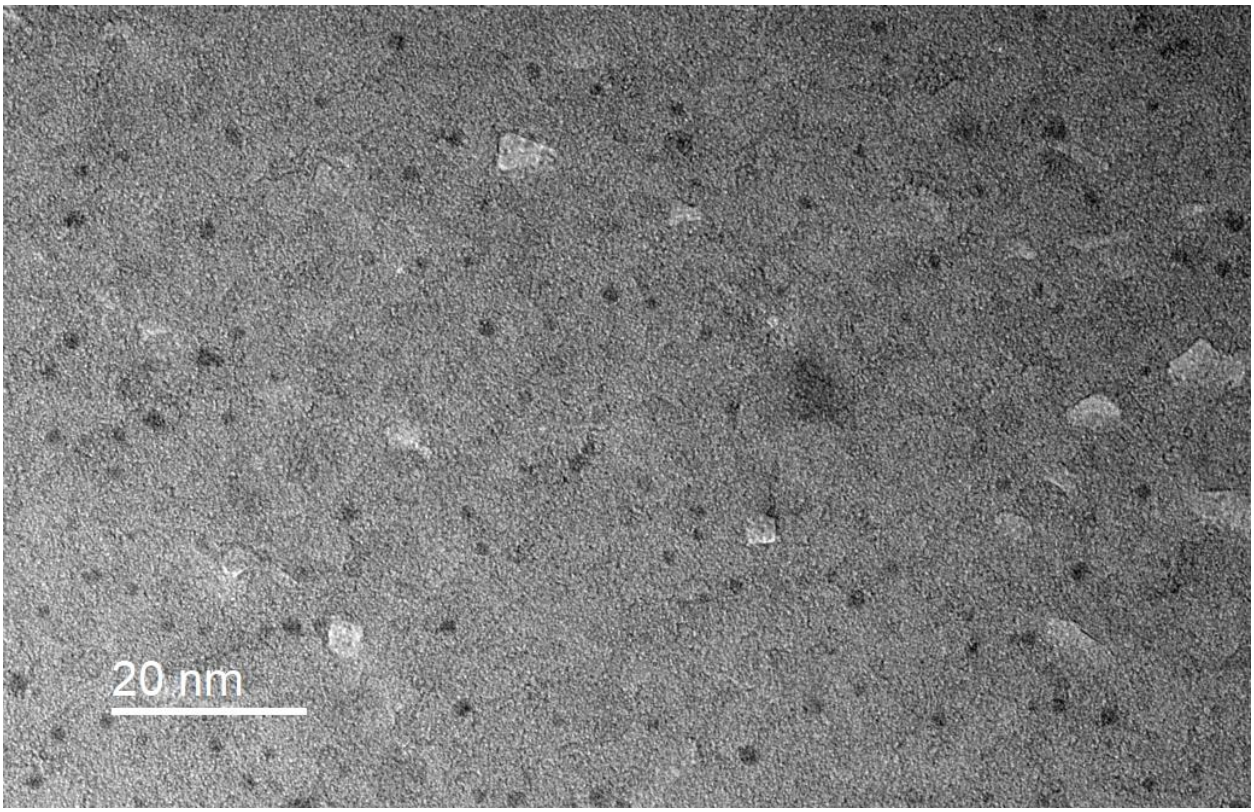

Figure S4. TEM image of size-selected Ag clusters, corresponding to the dark blue curve in Fig. 1 in the text.

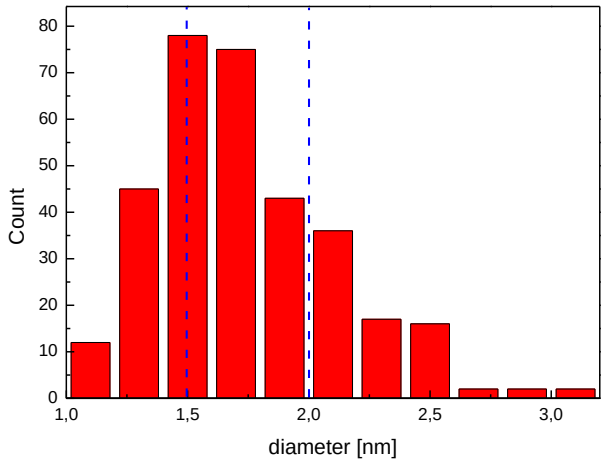

Figure S5. Diameter distribution obtained for the same sample as in Fig.S4. The dashed blue lines show the lower and upper limit of deposited size.

Description of matrix porosity in the simulations

The alumina films fabricated by electron beam evaporation are porous, we have in the past characterized them using ellipsometry to 70% density [3]. This has to be taken into account in the numerical simulations. Four different cases are used for the alumina matrix as effective dielectric medium: dense and porous alumina, with and without a thin layer of vacuum at the interface between metal and matrix. A thin vacuum layer (d = 2 Bohr, 1.06 Å) has been used in some of our earlier work as a different phenomenological description of matrix porosity [4, 5, 6].

In order to reasonably compare simulation and experiment, we plot in Fig. S6 the maxima of the experimental curves and the weighted means for the simulated spectra with δ = 60 meV, averaged between 1.8 and 3.8 eV, i.e. the onset of interband transitions. Choosing the weighted mean for the simulated spectra has proven better than fitting a single response function, especially for highly fragmented spectra. These values are plotted in the lower half of the figure.

From Fig. S6 we conclude that the best agreement between experiment and simulation is obtained for a continuous porous alumina matrix with the experimentally derived dielectric function (green triangles). Mimicking the local porosity with a vacuum layer at the interface yields values in the correct range but predicts a size-effect not observed in the experiment. The values obtained for a dense, non-porous matrix are consistently too low in energy by ~150 meV.

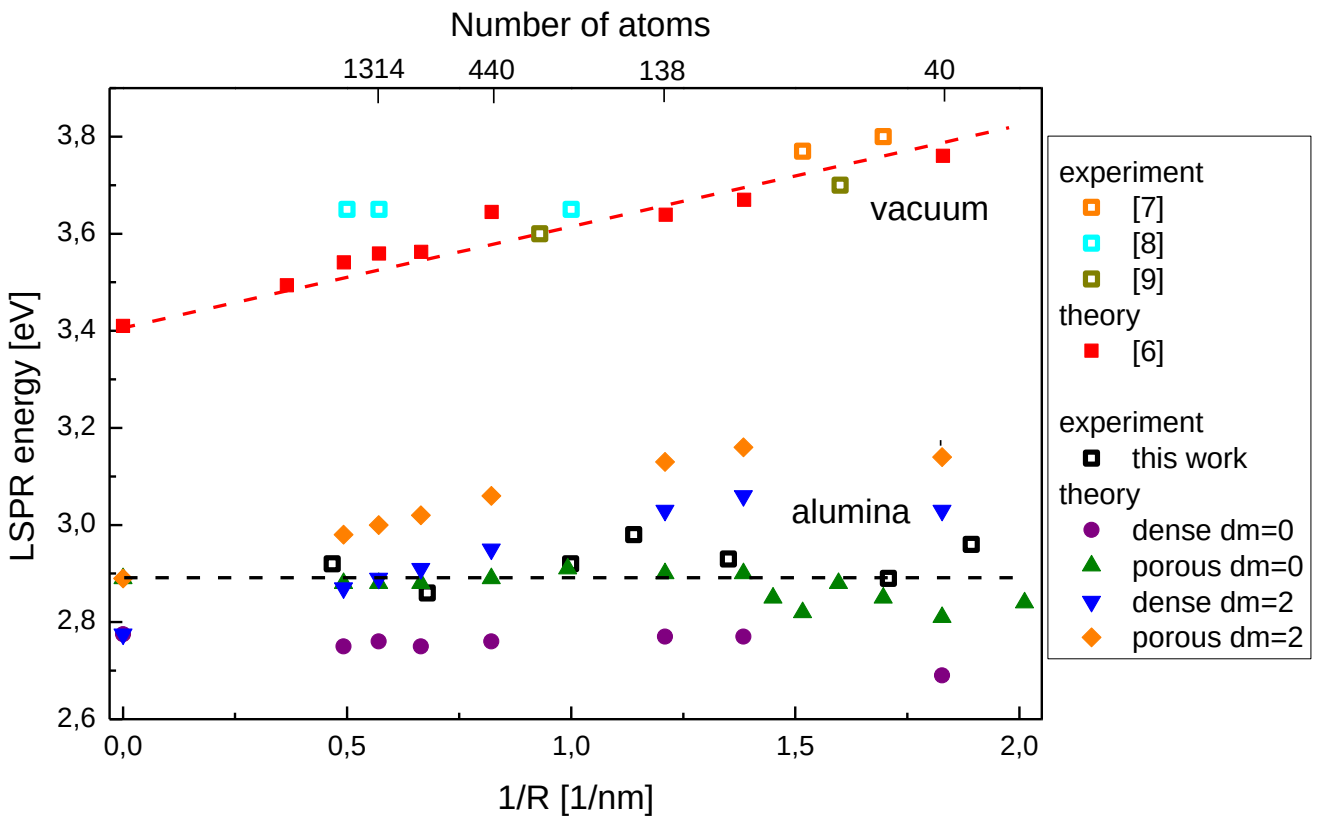

Figure S6. Comparison of mean LSPR energies. Experimental values are given by open squares, weighted means for different simulation series by solid symbols. At the top of the figure are displayed values for gas phase clusters, at the bottom for alumina-embedded ones. The reference numbers refer to those of the Supporting Information.

Also shown in Fig. S6 are experimental and theoretical values for gas phase clusters. Here we clearly see the influence of the environment on the mean plasmonic response and the relative scatter of simulated responses. The theoretical values are taken from [6], the experimental ones from [7, 8, 9]

We note furthermore that, in general, for the smallest sizes (below ~80 atoms), as the number of atoms in the cluster is reduced, corrections to our spherical jellium description might become

necessary. Whether the scatter of mean LSPR energies, as shown in Fig. S6, is real or due to an increasing insufficiency of the theoretical approach, has to be validated by ab-initio methods such as TD-DFT, which are today not available for oxide-embedded clusters. The scatter of the order of ~100 meV is much smaller than the environmental effects.

On the choice of the parameter δ in the simulations

In classical Mie theory in the quasi-static limit the width of the LSPR is defined by the dielectric function and no size dependence is considered [10]. Depending on the tables used for the optical constants, different values for the width are obtained. The table in [11] give a FWHM of <60 meV, whereas that of [12] give >160 meV (cf. Fig S7). These widths reflect the bulk dissipation due to collisions of electrons with other electrons, phonons, defects etc. To this intrinsic damping one has to add surface effects which are commonly modeled through an additive term proportional to 1/R, with R the cluster radius. The proportionality factor includes homogeneous contributions (Landau damping) as well as inhomogeneous ones, reflecting the averaged ensemble measurement. It thus strongly depends on the material, the environment and the experimental conditions, notably the matrix porosity and interface roughness. It is typically adjusted to fit the experimental data, see e.g. [13].

In our work we use atomistic input parameters to model the bulk part of the plasmonic response, analogous to a Mie description as described above: the electron effective mass (taken as 1), the Wigner-Seitz radius of bulk silver, the d-electron part of the dielectric function (taken from [12]) and an extrapolated value for the intrinsic damping constant Γ. This last has been determined by extrapolation to 120 meV, i.e. $\delta = 60$ meV [14]. With these values we obtain a classical Mie plasmon with FWHM = 100 eV, slightly lower than 120 meV because of dielectric screening effects, as detailed in [15] (eq. 3) and in between the values of Mie theory using [11, 12].

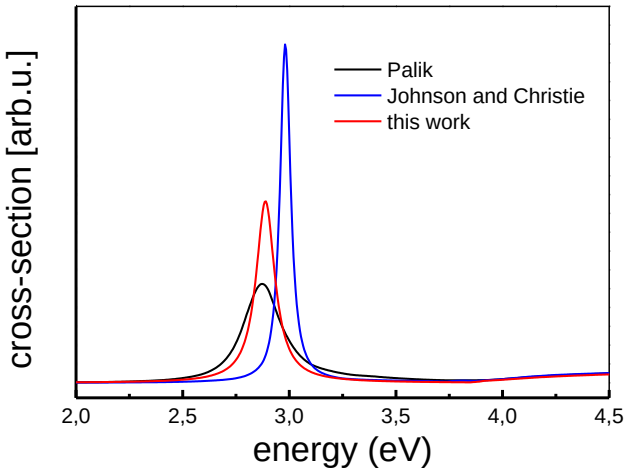

Figure S7. Simulated absorption cross sections using quasi-static Mie theory with the dielectric functions from refs. [11, 12]. Also shown is the curve using the model of this article in the large diameter limit. All curves are calculated with the experimental dielectric function of porous alumina, as described in the text.

In order to account for surface effects, Landau damping is included in our theoretical description. As described in the text, the delocalized conduction electrons, oscillating in the external field, probe the anharmonic part of the electron-jellium potential and thereby couple to internal single-electron excitations. Thus, the simulated spectra in Fig. 3 with $\delta = 60$ meV include Landau damping but do not include all inhomogeneous line broadening effects due to interface inhomogeneities etc. These last are then added empirically by using increased values for δ. The combination of these two then corresponds to the phenomenological description with the 1/R correction, as described above.

Simulated absorption spectra

In the following are shown the simulated absorption spectra for given sizes of n silver atoms and embedded in alumina matrices with different descriptions of porosity. In all cases the thickness of the layer of reduced d electron polarizability was fixed to d = 3.5 bohr, consistently with all our past work, and the intrinsic line width taken as 2δ = 120 meV.

In the left column are displayed the spectra using the dielectric function of bulk alumina as taken from [12] in black curves and those of porous alumina with the experimental values of [3] in red. In both cases d_m is taken as zero, corresponding to a neat interface between metal and matrix.

In the right column are shown the spectra with the same two dielectric functions, but this time with a thin layer of vacuum of d_m = 2 bohr (1.06 Å) thickness at the metal-matrix interface, mimicking local matrix porosity.

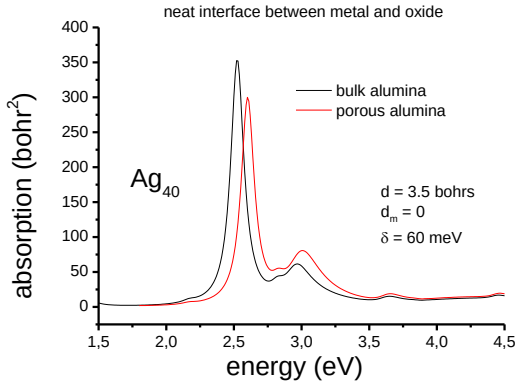

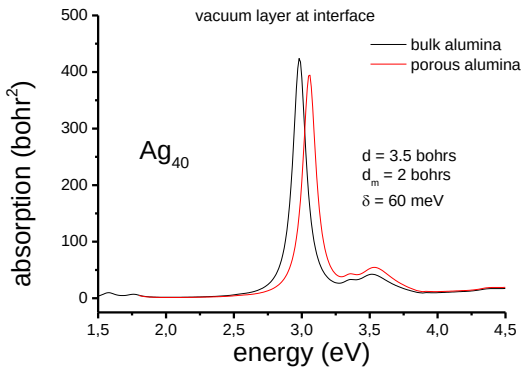

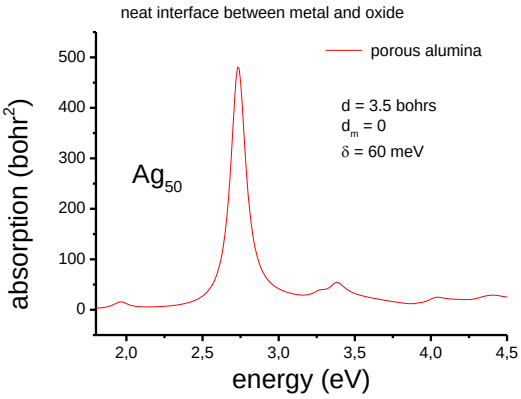
neat interface between metal and oxide
porous alumina
d = 3.5 bohrs
d_m = 0
δ = 60 meV
Ag_{50}
absorption (bohr^2)
energy (eV)
0
100
200
300
400
500
2,0
2,5
3,0
3,5
4,0
4,5

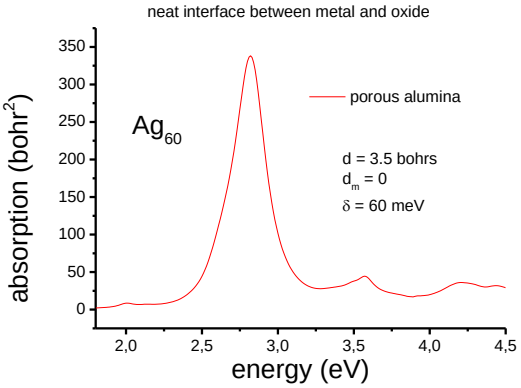
neat interface between metal and oxide
porous alumina
d = 3.5 bohrs
d_m = 0
δ = 60 meV
Ag_{60}
absorption (bohr^2)
energy (eV)
0
50
100
150
200
250
300
350
2,0
2,5
3,0
3,5
4,0
4,5

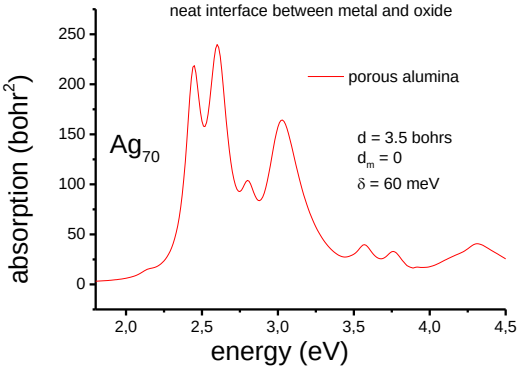
neat interface between metal and oxide
porous alumina
d = 3.5 bohrs
d_m = 0
δ = 60 meV
Ag_{70}
absorption (bohr^2)
energy (eV)
0
50
100
150
200
250
2,0
2,5
3,0
3,5
4,0
4,5

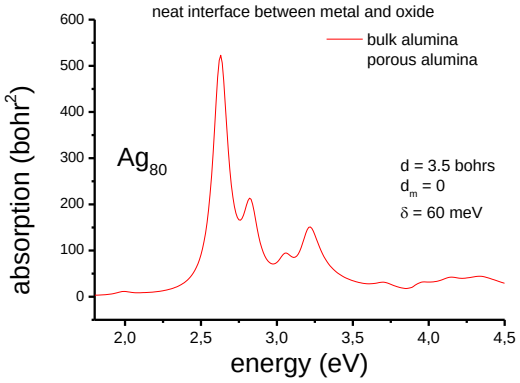
neat interface between metal and oxide
bulk alumina
porous alumina
Ag80
d = 3.5 bohrs
dm = 0
δ = 60 meV
absorption (bohr2)
energy (eV)

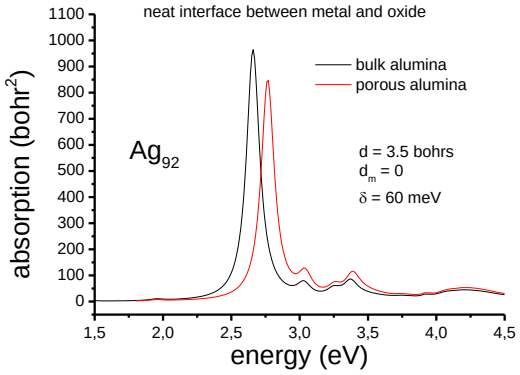
neat interface between metal and oxide
bulk alumina
porous alumina
Ag92
d = 3.5 bohrs
dm = 0
δ = 60 meV
absorption (bohr2)
energy (eV)

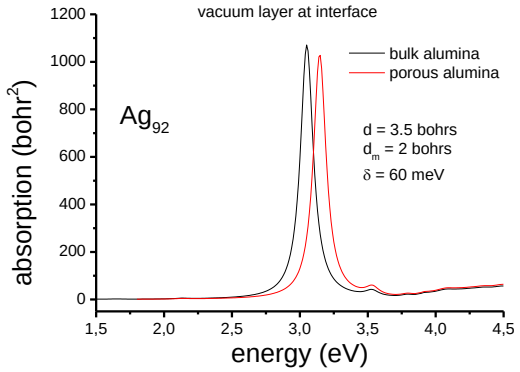
vacuum layer at interface
bulk alumina
porous alumina
Ag92
d = 3.5 bohrs
dm = 2 bohrs
δ = 60 meV
absorption (bohr2)
energy (eV)

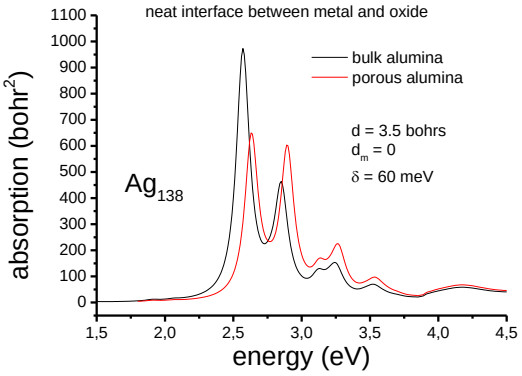
neat interface between metal and oxide
bulk alumina
porous alumina
Ag138
d = 3.5 bohrs
dm = 0
δ = 60 meV
absorption (bohr2)
energy (eV)

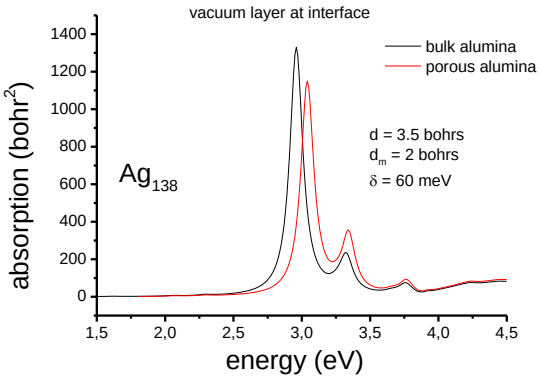
vacuum layer at interface
bulk alumina
porous alumina
Ag138
d = 3.5 bohrs
dm = 2 bohrs
δ = 60 meV
absorption (bohr2)
energy (eV)

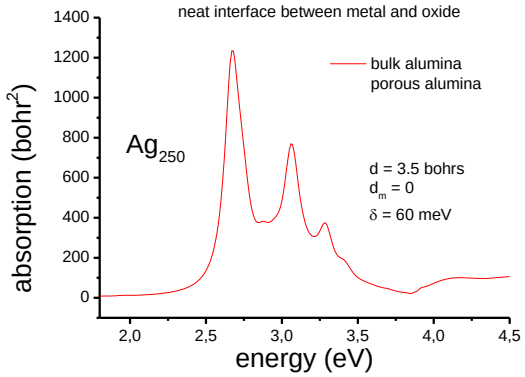
neat interface between metal and oxide
bulk alumina
porous alumina
Ag250
d = 3.5 bohrs
dm = 0
δ = 60 meV
absorption (bohr2)
energy (eV)

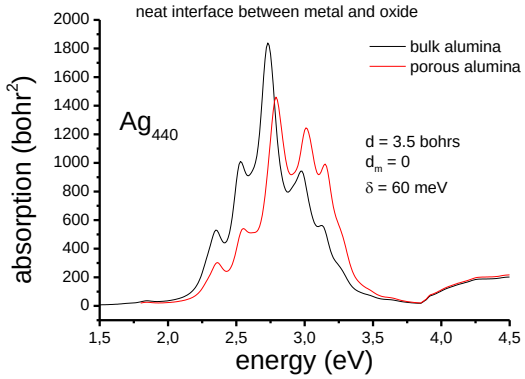
neat interface between metal and oxide
bulk alumina
porous alumina
Ag440
d = 3.5 bohrs
dm = 0
δ = 60 meV
absorption (bohr2)
energy (eV)

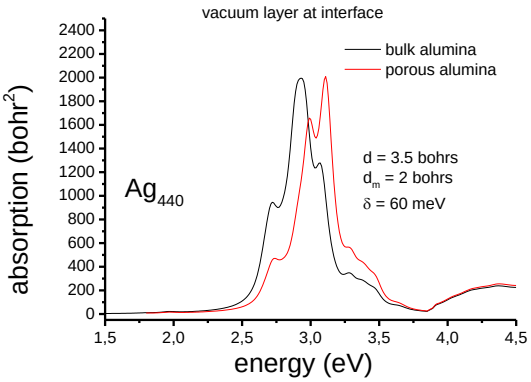
vacuum layer at interface
bulk alumina
porous alumina
Ag440
d = 3.5 bohrs
dm = 2 bohrs
δ = 60 meV
absorption (bohr2)
energy (eV)

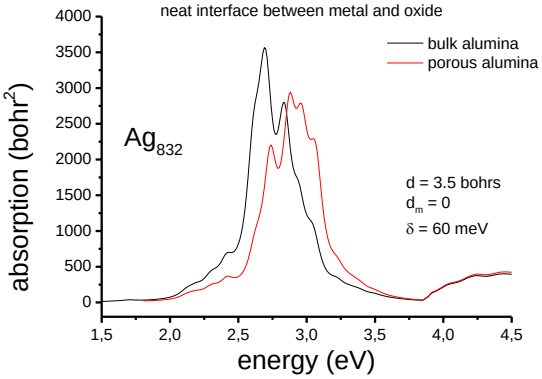
neat interface between metal and oxide
bulk alumina
porous alumina
Ag832
d = 3.5 bohrs
dm = 0
δ = 60 meV
absorption (bohr2)
energy (eV)

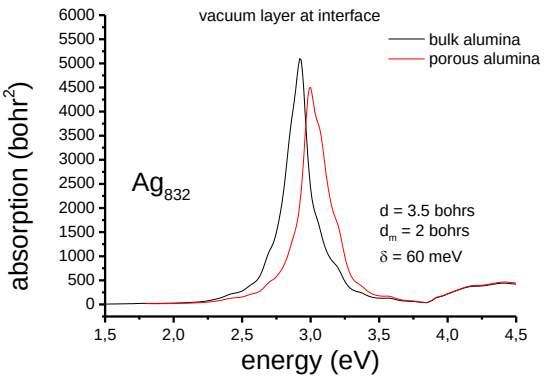
vacuum layer at interface
bulk alumina
porous alumina
Ag832
d = 3.5 bohrs
dm = 2 bohrs
δ = 60 meV
absorption (bohr2)
energy (eV)

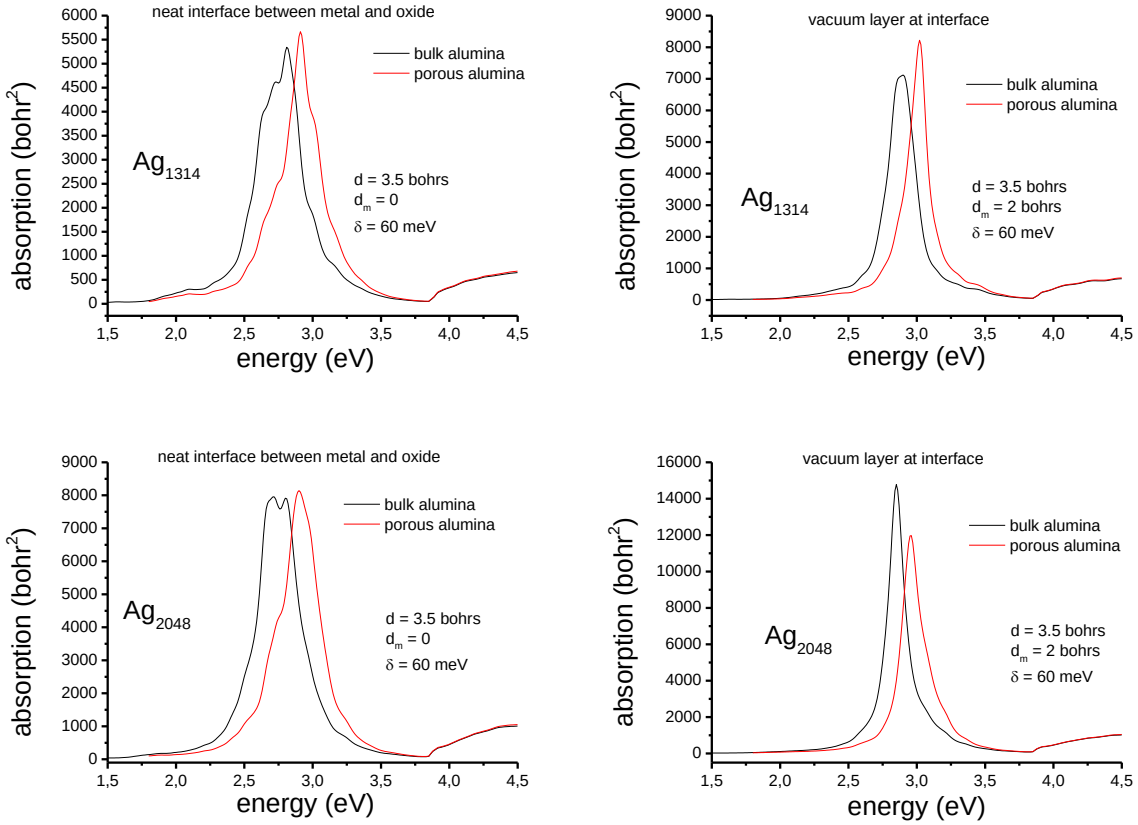

REFERENCES

[1] Alayan, R., Arnaud, L., Bourgey, A., Broyer, M., Cottancin, E., Huntzinger, J. R., Lermé, J., Vialle, J. L., Pellarin, M., and Guiraud, G. Application of a static quadrupole deviator to the deposition of size-selected cluster ions from a laser vaporization source. *Rev. Sci. Instrum.* **75**, 2461 (2004).

[2] Oyarzún, S., Tamion, A., Tournus, F., Dupuis, V., and Hillenkamp, M. Size effects in the magnetic anisotropy of embedded cobalt nanoparticles: from shape to surface. *Sci. Rep.* **5**, 14749 (2015).

[3] Palpant, B., Prével, B., Lermé, J., Cottancin, E., Pellarin, M., Treilleux, M., Perez, A., Vialle, J. L., and Broyer, M. Optical properties of gold clusters in the size range 2-4 nm. *Phys. Rev. B* **57**, 1963 (1998).

[4] Lermé, J., Palpant, B., Prével, B., Pellarin, M., Treilleux, M., Vialle, J. L., Perez, A., and Broyer, M. Quenching of the Size Effects in Free and Matrix-Embedded Silver Clusters. *Phys. Rev. Lett.* **80**(23), 5105–5108 (1998).

[5] Lermé, J. Introduction of quantum finite-size effects in the Mie's theory for a multilayered metal sphere in the dipolar approximation: Application to free and matrix-embedded noble metal clusters. *Eur. Phys. J. D* **10**(2), 265–277 (2000).

[6] Campos, A., Troc, N., Cottancin, E., Pellarin, M., Weissker, H.-C., Lermé, J., Kociak, M., and Hillenkamp, M. Plasmonic Quantum Size Effects in Silver Nanoparticles are Dominated by Interfaces and Local Environments. *Nat. Phys.* **15**, 275–280 (2019).

[7] Tiggesbäumker, J., Köller, L., Meiwes-Broer, K.-H., and Liebsch, A. Blue shift of the Mie plasma frequency in Ag clusters and particles. *Phys. Rev. A* **48**, R1749–R1752 (1993).

[8] Hilger, A., Cüppers, N., Tenfelde, M., and Kreibig, U. Surface and interface effects in the optical properties of silver nanoparticles. *Eur. Phys. J. D* **10**, 115–118 (2000).

[9] Loginov, E., Gomez, L. F., Chiang, N., Halder, A., Guggemos, N., Kresin, V. V., and Vilesov, A. F. Photoabsorption of Ag_N (N~6-6000) Nanoclusters Formed in Helium Droplets: Transition from Compact to Multicenter Aggregation. *Phys. Rev. Lett.* **106** (2011).

[10] Kreibig, U. and Vollmer, M. *Optical properties of metal clusters*. Springer series in materials science. Springer Berlin, (1995).

[11] Johnson, P. B. and Christy, R. W. Optical Constants of the Noble Metals. *Phys. Rev. B* **6**, 4370–4379 (1972).

[12] Palik, E. *Handbook of Optical Constants of Solids*. Academic, New York, (1985).

[13] Hövel, H., Fritz, S., Hilger, A., Kreibig, U., and Vollmer, M. Width of cluster plasmon resonances: Bulk dielectric functions and chemical interface damping. *Phys. Rev. B* **48**(24), 18178–88 (1993).

[14] Baida, H., Billaud, P., Marhaba, S., Christofilos, D., Cottancin, E., Crut, A., Lermé, J., Maioli, P., Pellarin, M., Broyer, M., Del Fatti, N., Vallée, F., Sánchez-Iglesias, A., Pastoriza-Santos, I., and Liz-Marzán, L. M. Quantitative Determination of the Size Dependence of Surface Plasmon Resonance Damping in Single Ag@SiO_2 Nanoparticles. *Nano Letters* **9**(10), 3463–3469 (2009). PMID: 19719148.

[15] Lermé, J. Size Evolution of the Surface Plasmon Resonance Damping in Silver Nanoparticles: Confinement and Dielectric Effects. *J. Phys. Chem. C* **115**(29), 14098–14110 (2011).